

# NUMERICAL SIMULATION OF CARREAU FLOWS THROUGH AN ABRUPT CONTRACTION BY A GALERKIN LEAST-SQUARES METHODOLOGY

**Renato Martins, martins@mecanica.ufrgs.br, Filipe Silveira, fsilveira@mecanica.ufrgs.br**

Laboratory of Computational and Applied Fluid Mechanics (LAMAC), Mechanical Engineering Department, Universidade Federal do Rio Grande do Sul

**Maria Laura Martins Costa, laura@mec.uff.br**

Laboratory of Theoretical and Applied Mechanics (LMTA), Mechanical Engineering Department – PGMEC, Universidade Federal Fluminense

**Sérgio Frey, frey@mecanica.ufrgs.br**

Laboratory of Computational and Applied Fluid Mechanics (LAMAC), Mechanical Engineering Department, Universidade Federal do Rio Grande do Sul

**Abstract.** *This article presents a finite element simulation of Carreau flows through an abrupt contraction. The employed mechanical model consists in using the Carreau viscosity equation to characterize the shear-thinning fluid behavior, giving rise to a generalization of Navier-Stokes equation containing a non-linear diffusion term. A Galerkin-Least Squares methodology approximates the mechanical model circumventing the Babuška-Brezzi condition, which consists of adding to the classical Galerkin method mesh-dependent residuals, resulting from a least-squares minimization of the Euler-Lagrange equations of the problem. These perturbation terms are built in to enhance stability of original Galerkin formulation without upsetting the problem consistency. Numerical results for both velocity and pressure fields accounting for shear-rate dependent viscosity have been obtained for an axisymmetric 4:1 sudden contraction with Carreau number ranging from 0 to 100, Reynolds number from 2 to 100 and power-law exponent from 0.2 to 1.0. These results have shown good agreement with the literature.*

**Keywords:** *Non-Newtonian fluids; Shear-thinning, Carreau fluid; sudden contraction flow; Galerkin least-squares method.*

## 1. INTRODUCTION

Non-Newtonian fluid behavior is present in a wide class of fluids, many of them exhibiting shear-thinning effect. Kim *et al.* (1983) have employed a classical finite element approach to study the roles of fluid inertia and shear-rate dependence of a Carreau viscosity field, concluding that effect of increasing either shear-thinning or fluid inertia decreases the upstream vortex size at the sudden contraction flow. Fang *et al.* (1999) employed a finite difference scheme to model laminar fully-developed flows in an eccentric annular geometry for power-law fluids. Reis Junior and Naccache (2003) simulated, via a finite volume methodology, non-Newtonian fluids through axisymmetric sudden expansion and contraction flows, investigating the influence of rheological parameters on these flows. Neofytou (2005) also employed a finite volume methodology, employing the SIMPLE pressure-correction strategy coupled to the QUICK difference scheme, to simulate four non-Newtonian viscous models in a lid-driven cavity flow: power-law, Quemada and modified Bingham and Casson ones.

In the present work a Galerkin/least-squares (GLS) methodology was employed to simulate Carreau flows through an axisymmetric 4:1 sudden contraction, accounting for fluid inertia and shear-rate dependency on viscosity. This GLS methodology overcomes classical Galerkin shortcomings at high advective flows by adding mesh-dependent terms (functions of the residuals of the Euler-Lagrange equations evaluated elementwise) to classical Galerkin formulation, enhancing its convergence without upsetting its consistency, since the residuals of the Euler-Lagrange equations are satisfied by their exact solutions. Stabilization is important not only to circumvent Babuška-Brezzi condition but also to preserve numerical stability in locally advective dominated flow regions due to the material behavior of shear-thinning liquids.

In all numerical simulations, a structured non-uniform finite element mesh has been employed, consisting of 7,154 equal-order bilinear quadrilateral elements (Q1/Q1), in order to approximate velocity and pressure fields. The Carreau number was investigated from 0 to 100, the shear-thinning coefficient from 0.2 to 1.0 and the Reynolds number from 2 to 100.

## 2. MECHANICAL MODEL AND NUMERICAL FORMULATION

The mechanical model employs the continuity and motion equations to simulate steady-state isothermal axisymmetric flows of inelastic incompressible fluids, considering Cauchy stress tensor:  $\boldsymbol{\sigma} = -p\mathbf{I} + \boldsymbol{\tau}$ , where  $p$  is a mean pressure and  $\boldsymbol{\tau}$  the deviatoric stress, being given by:

$$\begin{aligned}
 r^{-1} \partial_r (r u_r) + \partial_z u_z &= 0 \\
 \rho (\partial_t u_r + u_r \partial_r u_r + u_z \partial_z u_r) &= -\partial_r p + r^{-1} [\partial_r (r \tau_{rr}) - \tau_{\theta\theta}] + \partial_z \tau_{rz} + \rho f_r \\
 \rho (\partial_t u_z + u_r \partial_r u_z + u_z \partial_z u_z) &= -\partial_z p + r^{-1} \partial_r (r \tau_{rz}) + \partial_z \tau_{zz} + \rho f_z
 \end{aligned} \tag{1}$$

where  $u_r$  and  $u_z$  are the non-zero components of the fluid velocity,  $\rho$  its mass density,  $\tau_{rr}$ ,  $\tau_{rz}$ ,  $\tau_{zr}$ ,  $\tau_{\theta\theta}$  and  $\tau_{zz}$ , are the non-zero components of the deviatoric stress tensor and  $\rho f_r$  and  $\rho f_z$  represent the radial and axial components of the body force per unit mass.

A non-linear dependence of the deviatoric stress on the rate of strain tensor may be introduced by considering a generalized Newtonian constitutive law  $\boldsymbol{\tau}(\dot{\boldsymbol{\gamma}}) = 2\eta(\dot{\boldsymbol{\gamma}})\mathbf{D}(\mathbf{u})$  with  $\mathbf{D}$  being the symmetric portion of the velocity gradient – denoted by rate of strain tensor – and  $\eta(\dot{\boldsymbol{\gamma}})$  is the shear rate viscosity. For an axisymmetric flow, the components of the deviatoric stress tensor may be expressed as

$$\begin{aligned}
 \tau_{rr} &= 2\eta(\dot{\boldsymbol{\gamma}})\partial_r u_r \\
 \tau_{\theta\theta} &= 2\eta(\dot{\boldsymbol{\gamma}})r^{-1}u_r \\
 \tau_{zz} &= 2\eta(\dot{\boldsymbol{\gamma}})\partial_z u_z \\
 \tau_{zr} &= \eta(\dot{\boldsymbol{\gamma}})(\partial_z u_r + \partial_r u_z)
 \end{aligned} \tag{2}$$

In the present work the viscosity function  $\eta(\dot{\boldsymbol{\gamma}})$  is given by Carreau constitutive equation (Bird *et al.*, 1987)

$$\frac{\eta - \eta_\infty}{\eta_0 - \eta_\infty} = [1 + (\lambda \dot{\boldsymbol{\gamma}})^2]^{(n-1)/2} \tag{3}$$

with  $\eta_0$  and  $\eta_\infty$  being asymptotic values of fluid viscosity at zero and infinite shear rates, respectively,  $\lambda$  being a characteristic time equal to the reciprocal of the shear rate at which shear thinning begins and, finally,  $(n-1)$  represents the power-law slope of the logarithmic of viscosity function,  $\eta(\dot{\boldsymbol{\gamma}})$ . The shear rate scalar,  $\dot{\boldsymbol{\gamma}}$ , represents the Frobenius norm of tensor  $\mathbf{D}$ , a mathematical measure for the shear rate when simple shear flow is assumed – namely:  $\dot{\boldsymbol{\gamma}} = (2 \text{tr } \mathbf{D}^2)^{1/2}$ .

Taking the mass and momentum balance equations, Eq.(1), for an inelastic incompressible fluid on steady-state isothermal axisymmetric flow, coupled with the Carreau constitutive model, Eq.(3), the following boundary value problem may be stated:

$$\begin{aligned}
 \rho (u_r \partial_r u_r + u_z \partial_z u_r) &= -\partial_r p + r^{-1} [\partial_r (2\eta(\dot{\boldsymbol{\gamma}})\partial_r u_r) - 2\eta(\dot{\boldsymbol{\gamma}})r^{-1}u_r] \\
 &\quad + \partial_z \eta(\dot{\boldsymbol{\gamma}})(\partial_z u_r + \partial_r u_z) + \rho f_r && \text{in } \Omega \\
 \rho (u_r \partial_r u_z + u_z \partial_z u_z) &= -\partial_z p + r^{-1} \partial_r [r \eta(\dot{\boldsymbol{\gamma}})(\partial_z u_r + \partial_r u_r)] \\
 &\quad + \partial_z (2\eta(\dot{\boldsymbol{\gamma}})\partial_z u_z) + \rho f_z && \text{in } \Omega \\
 r^{-1} \partial_r (r u_r) + \partial_z u_z &= 0 && \text{in } \Omega \\
 u_r &= u_{g_r} && \text{on } \Gamma_{g_r} \\
 u_z &= u_{g_z} && \text{on } \Gamma_{g_z} \\
 -p + 2\eta(\dot{\boldsymbol{\gamma}})\partial_r u_r &= t_{h_r} && \text{on } \Gamma_{h_r} \\
 \eta(\dot{\boldsymbol{\gamma}})(\partial_z u_r + \partial_r u_z) &= t_{h_z} && \text{on } \Gamma_{h_z}
 \end{aligned} \tag{4}$$

Equation (4) is stated considering an internal domain  $\Omega \subset \mathbb{R}^2$  with a polygonal or polyhedral boundary  $\Gamma$ , formed by the union of  $\Gamma_g$  – the portion of  $\Gamma$  where Dirichlet conditions are imposed – and  $\Gamma_h$  – the portion subjected to Neumann boundary conditions. In this equation  $t_{h_r}$  and  $t_{h_z}$  are the non-zero components of the stress vector on  $\Gamma_{h_r}$  and  $\Gamma_{h_z}$ , respectively.

### 3. GALERKIN LEAST-SQUARES FORMULATION

The finite element approximation of Eq. (4) was built in by employing the usual fluid dynamics subspaces for velocity ( $\mathbf{V}_h$ ) and pressure ( $P_h$ ) (Ciarlet, 1978),

$$\begin{aligned}
 V_h &= \{ \mathbf{v} \in H_1^0(\Omega)^N | \mathbf{v}|_K \in R_k(\Omega_K)^N, K \in \Omega_h \} \\
 P_h &= \{ p \in C^0(\Omega) \cap L_0^2(\Omega) | p|_K \in R_l(\Omega_K), K \in \Omega_h \} \\
 V_h^g &= \{ \mathbf{v} \in H_1^0(\Omega)^N | \mathbf{v}|_K \in R_k(\Omega_K), K \in \Omega^k, \mathbf{v}_i = \mathbf{u}_g \text{ on } \Gamma_g \}
 \end{aligned} \tag{5}$$

with  $R_m$  ( $m=k,l$ ) denoting the polynomial spaces of degree  $m$ ,  $\Omega_h$  a usual finite element partitioning (Ciarlet, 1978) and  $\Omega_K$  the domain of the  $K$ -finite element of  $\Omega_h$ .

Based on the above definitions of velocity and pressure subspaces, Eq. (5), a Galerkin least-squares formulation for the problem presented in Eq. (4) may be stated as: *Find the pair  $(\mathbf{u}^h, p^h) \in \mathbf{V}_h^g \times P_h$ , such that, for all  $(\mathbf{v}^h, q^h) \in \mathbf{V}_h \times P_h$ :*

$$\begin{aligned}
 & \int_{\Omega} \rho (u_r^h \partial_r u_r^h + u_z^h \partial_z u_r^h) v_r^h d\Omega + \int_{\Omega} \rho (u_r^h \partial_r u_z^h + u_z^h \partial_z u_z^h) v_z^h d\Omega \\
 & - \int_{\Omega} p^h [r^{-1} \partial_r (r v_r^h) + \partial_z v_z^h] d\Omega - \int_{\Omega} [r^{-1} \partial_r (r u_r^h) + \partial_z u_z^h] q^h d\Omega \\
 & + \int_{\Omega} 2\eta(\dot{\gamma}) [\partial_z (\partial_z u_r^h + \partial_r u_z^h) / 2 + r^{-1} (\partial_r (r \partial_r u_r^h) - u_r^h / r)] \\
 & \quad \times [\partial_z (\partial_z v_r^h + \partial_r v_z^h) / 2 + r^{-1} (\partial_r (r \partial_r v_r^h) - v_r^h / r)] d\Omega \\
 & + \int_{\Omega} 2\eta(\dot{\gamma}) [r^{-1} \partial_r r (\partial_z u_r^h + \partial_r u_z^h) / 2 + \partial_z \partial_z u_z^h] \\
 & \quad \times [\partial_z \partial_z v_z^h + r^{-1} \partial_r r (\partial_z v_r^h + \partial_r v_z^h) / 2] d\Omega \\
 & + \sum_{K \in \Omega_h} \int_{\Omega_K} [\rho (u_r^h \partial_r u_r^h + u_z^h \partial_z u_r^h) + \partial_r p^h - 2\eta(\dot{\gamma}) [r^{-1} (\partial_r (r \partial_r u_r^h) - u_r^h / r) + \partial_z (\partial_z u_r^h + \partial_r u_z^h) / 2]] \\
 & \quad \times \tau(\text{Re}_K) [\rho (u_r^h \partial_r v_r^h + u_z^h \partial_z v_r^h) - \partial_r q^h + 2\eta(\dot{\gamma}) [r^{-1} (\partial_r (r \partial_r v_r^h) - v_r^h / r) + \partial_z (\partial_z v_r^h + \partial_r v_z^h) / 2]] d\Omega \\
 & + \sum_{K \in \Omega_h} \int_{\Omega_K} [\rho (u_r^h \partial_r u_z^h + u_z^h \partial_z u_z^h) + \partial_z p^h - 2\eta(\dot{\gamma}) [r^{-1} (\partial_r (r \partial_z u_r^h + \partial_z u_z^h) / 2) + \partial_z \partial_z u_z^h]] \\
 & \quad \times \tau(\text{Re}_K) [\rho (u_r^h \partial_r v_z^h + u_z^h \partial_z v_z^h) - \partial_z q^h + 2\eta(\dot{\gamma}) [r^{-1} \partial_r (r \partial_z v_r^h + \partial_r v_z^h) / 2 + \partial_z \partial_z v_z^h]] d\Omega \\
 & = \int_{\Omega} \rho (f_r v_r + f_z v_z) d\Omega + \int_{\Gamma} (-p^h + 2\eta(\dot{\gamma}) \partial_r u_r^h) v_r^h d\Gamma + \int_{\Gamma} \eta(\dot{\gamma}) (\partial_z u_r^h + \partial_r u_z^h) v_z^h d\Gamma \\
 & + \sum_{K \in \Omega_h} \int_{\Omega_K} \rho f_r \tau(\text{Re}_K) [(u_r^h \partial_r v_r^h + u_z^h \partial_z v_r^h) - \partial_r q^h + 2\eta(\dot{\gamma}) [\partial_z (\partial_z v_r^h + \partial_r v_z^h) / 2 + r^{-1} (\partial_r (r \partial_r v_r^h) - v_r^h / r)]] d\Omega \\
 & + \sum_{K \in \Omega_h} \int_{\Omega_K} \rho f_z \tau(\text{Re}_K) [(u_r^h \partial_r v_z^h + u_z^h \partial_z v_z^h) - \partial_z q^h + 2\eta(\dot{\gamma}) [\partial_z \partial_z v_z^h + r^{-1} \partial_r r (\partial_z v_r^h + \partial_r v_z^h) / 2]] d\Omega
 \end{aligned} \tag{6}$$

in which the stability parameter  $\tau(\text{Re}_K)$  is defined as:

$$\begin{aligned}
 \tau(\text{Re}_K) &= \frac{h_K}{2|\mathbf{u}|_p} \xi(\text{Re}_K); \quad \text{with} \quad \xi(\text{Re}_K) = \text{Re}_K, \text{ for } 0 \leq \text{Re}_K < 1 \text{ or } \xi(\text{Re}_K) = 1, \text{ for } \text{Re}_K > 1 \\
 & \quad \text{and} \quad \text{Re}_K = \frac{m_K \rho |\mathbf{u}|_p h_K}{4\eta(\dot{\gamma})}
 \end{aligned} \tag{7}$$

with  $|\mathbf{u}|_p$  denoting the  $p$ -norm on  $\mathbb{R}^n$  and the parameter  $m_K$  being determined from the error analysis introduced by Franca and Frey (1992).

*Remark:* When the parameter  $\tau(\text{Re}_K)$  is equal to zero in the GLS formulation defined in Eq. (6)-(7), the classical Galerkin formulation is recovered.

#### 4. NUMERICAL RESULTS

The computational implementation of the GLS formulation has been validated by the benchmark of the lid-driven cavity problem for Newtonian fluids subjected to high advection flows. The cavity layout consists of a bi-unity cavity with a moving lid with impermeability and no-slip boundary condition at its walls, except for the lid at the superior edge which moves with a steady horizontal prescribed velocity – see, for instance Neofytou (2005), for problem statement details. A uniform finite element partitioning of the computational domain in 130x130 quadrilateral bilinear elements (Q1/Q1) has been considered in the usual way (Ciarlet, 1978), generating 17,161 nodal points. Three distinct Reynolds number were investigated, namely  $\text{Re}=1$  (for simulating creeping flows), 400 and 1000. All the computations have been performed with the finite element code for fluids under development at Laboratory of Computational and Applied Fluid Mechanics (LAMAC-UFRGS).

Figures 1 and 2 show the comparison between GLS approximations obtained in this work and those by Ghia *et al.* (1982) including inertia effects – namely  $\text{Re}=400$  e  $\text{Re}=1000$  – as well as with results from Jurjevic (1999) for creeping

flow ( $Re=1$ ). The horizontal profile – at  $x=0.5$  (Fig. 1) – and the vertical profile – at  $y=0.5$  (Fig. 2) – have shown good agreement with both articles for the investigated Reynolds numbers.

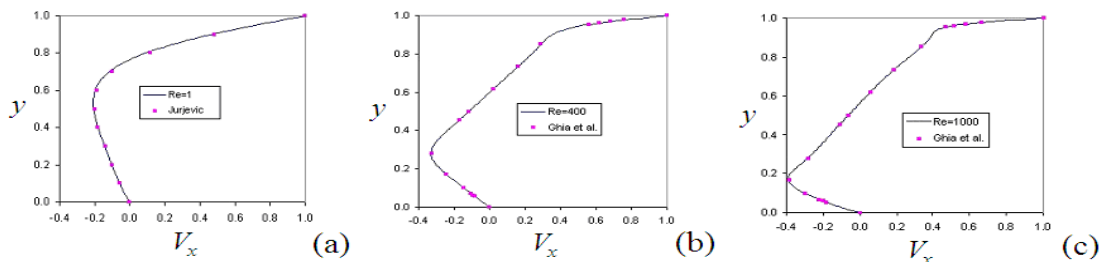


Figure 1: Lid-driven cavity flow – horizontal velocity profiles at  $x=0.5$ : (a)  $Re=1$ ; (b)  $Re=400$ ; (c)  $Re=1000$ .

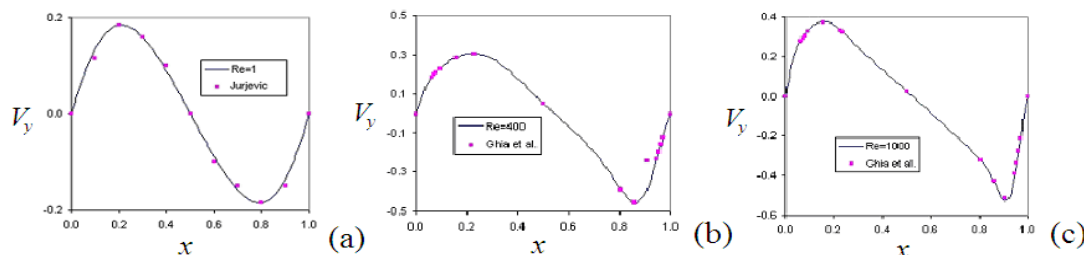


Figure 2: Lid-driven cavity flow – vertical velocity profiles at  $y=0.5$ : (a)  $Re=1$ ; (b)  $Re=400$ ; (c)  $Re=1000$ .

After validating the code, the GLS approximation defined in Eq.(6)-(7) has been implemented to simulate a Carreau (Eq. 3), flow through an axisymmetric 4:1 sudden contraction. The geometry was built in by joining a cylinder of radius  $R_1$  and length  $L_1$  with another one of smaller radius  $R_2$  and length  $L_2$ . The geometric configuration is mathematically described by the aspect ratio  $\beta=R_1/R_2$ . All simulated cases have employed  $\beta=4$ , as shown in Figure 3(a).

The imposed boundary conditions were: no-slip and impermeability at walls, symmetry velocity condition at the centerline; at the inlet a flat velocity profile was imposed while at the outlet free traction condition was adopted. Besides, the pressure is fixed at the outlet in one point:  $p_{ref}=0$ .

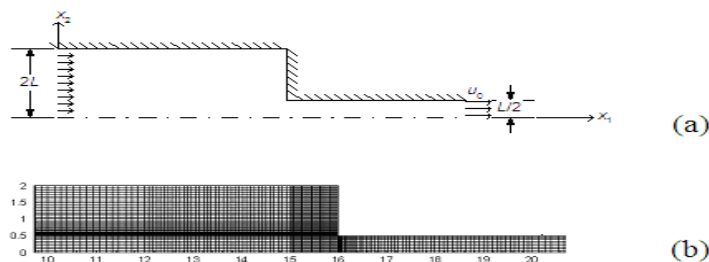


Figure 3: Axisymmetric sudden contraction flow: (a) problem statement; (b) detail of refined mesh at the contraction region.

After a mesh refining process ensuring mesh independence, the computational domain has been partitioned in the usual way (Ciarlet, 1978) into 7154 bilinear elements (Q1/Q1) – as depicted in Figure 3(b).

Reynolds number for this flow was defined considering the smaller radius cylinder  $R_2$ , its average velocity  $V_2$  and the zero-shear-rate viscosity  $\eta_0$ :

$$Re = \frac{2 R_2 \rho V_2}{\eta_0} \tag{8}$$

Introducing the Carreau number as

$$Cu = \frac{\lambda V_2}{R_2} \quad (9)$$

with the parameter  $\lambda$  defined as previously, and setting the infinite-shear-rate viscosity  $\eta_\infty=0$ , the Carreau viscosity equation (Eq. 3) may be redefined as

$$\eta(\dot{\gamma}) = [1 + (Cu \dot{\gamma})^2]^{(n-1)/2} \quad (10)$$

According to Eq.(10) a Newtonian behavior was recovered for  $Cu=0$  and the shear stress is given by

$$\tau(\dot{\gamma}) = \dot{\gamma} [1 + (Cu \dot{\gamma})^2]^{(n-1)/2} \quad (11)$$

Results investigating inertia effects have been obtained considering Reynolds number values varying from  $Re=2$  to  $Re=100$  – the former simulating negligible inertia flows. The shear-thinning effect has been investigated by considering distinct values of Carreau number – ranging from  $Cu=0$  to  $Cu=100$  – and by varying the power-law exponent from  $n=0.2$  to  $n=1.0$ .

In order to analyze the influence of Carreau number at the flow dynamics, at Figures 4 and 5 inertia effects have been neglected ( $Re=2$ ) and the power-law coefficient was fixed as  $n=0.2$ .

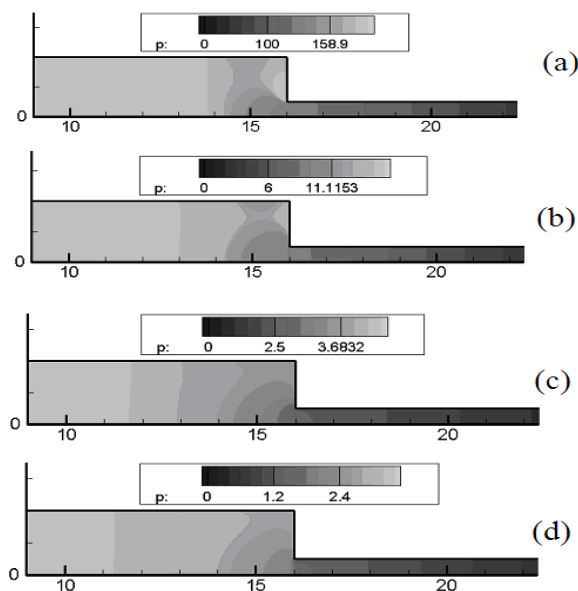


Figure 4. Pressure contours for  $n=2$  and  $Re=2$ : (a)  $Cu=0$ , (b)  $Cu=10$ , (c)  $Cu=50$  and (d)  $Cu=100$ .

Figure 4 presents pressure contours for  $Re=2$  and  $n=0.2$ . From all investigated  $Cu$  values it may be verified that an increase of Carreau number causes a monotonic decrease at pressure drop along the flow. This decrease is particularly accentuated for  $Cu$  between 0 (Figure 4(a) for  $Cu=0$ ) and 10 (Figure 4(b) for  $Cu=10$ ). Besides, for the highest values of  $Cu$  (Figure 4(c) for  $Cu=50$  and Figure 4(d) for  $Cu=100$ ), the pressure drop at the smaller tube is attenuated by shear-thinning effects. It is observed that the increase of Carreau number diminishes the fluid's resistance to flow and, consequently, the pressure drop.

Figure 5 presents a detail of the flow streamlines at the sudden contraction region, once again varying  $Cu$  from 0 to 100 and considering  $Re=2$  and  $n=0.2$ . For  $Cu=0$  – Newtonian case – a well-defined vortex is present at the contraction corner. This vortex tends to be collapsed as the shear-thinning effect becomes stronger, for  $Cu=50$  and  $Cu=100$  (Figures 5(c)-5(d)). As the shear thinning effect increases with Carreau number growth, the decreasing viscosity forces the flow at the larger tube to be locally advective dominated, giving rise to the vortex collapse.



Figure 5: A detail of flow streamlines at the sudden contraction region for  $n=2$  and  $Re=2$ : (a)  $Cu=0$ , (b)  $Cu=10$ , (c)  $Cu=50$  and (d)  $Cu=100$ .

Figure 6, also obtained by neglecting inertia effects, shows the influence of the power-law coefficient (ranging from  $n=0.2$  to  $n=1.0$ ) on the axial velocity profile at the contraction plane considering two distinct values of Carreau number – namely  $Cu=10$  in Figure 6(a) and  $Cu=100$  in Figure 6(b). Comparing both Figures 6(a) and 6(b), it may be noticed an increase of pseudoplasticity due to Carreau number augmentation, in which the power law index decrease causes the shear-thinning intensification. Figure 6 shows the evolution from the parabolic Newtonian profile ( $n=1$ ) to an almost flat profile ( $n=0.2$ ) – in both figures. This almost flat profile with very thin boundary layers near the walls – presenting severe velocity gradients, is characteristic of very strong shear-thinning, obtained by combining  $n=0.2$  and  $Cu=100$ . The deviation from the classical Newtonian pattern ( $n=1$ ) at the contraction plane results from the progressive decrease of viscosity related to the decrease of the power-law coefficient, being intensified by Carreau number augmentation. The concavity at the boundary layer edge for the strongest shear-thinning case ( $n=0.2$  and  $Cu=100$  – in Figure 6(b)) may be eliminated by employing shock-capture strategies (Galeão and Carmo, 1988).

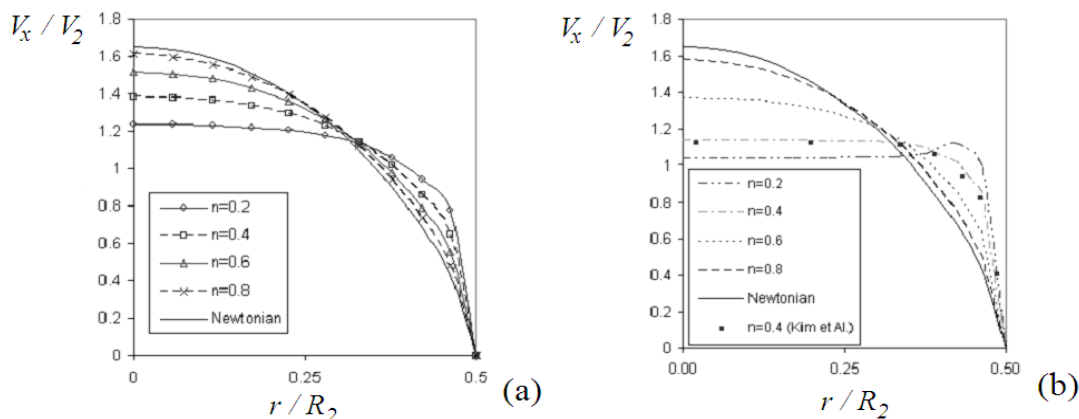


Figure 6: Axial velocity profiles at contraction plane for  $Re=2$  and distinct values of  $n$ : (a)  $Cu=10$  and (b)  $Cu=100$ .

Further, Figure 6(b) presents a comparison between results obtained in the present work for  $n=0.4$  and those by Kim *et al.* (1983). These authors have employed a classical Galerkin finite element approximation with a very coarse mesh, consisting of 116 Q2/Q1 elements. As observed from this figure both results show an excellent agreement.

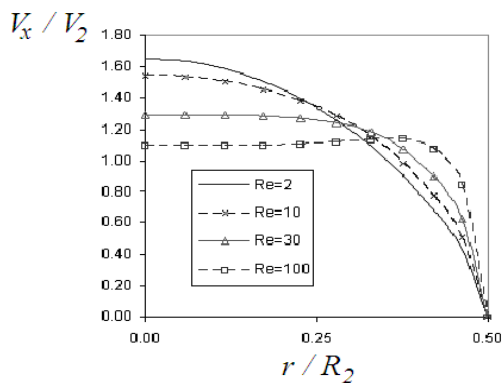


Figure 7: Radial velocity profiles for distinct Reynolds numbers and  $Cu=0$  at contraction plane.

In order to investigate the influence of the inertia effects on the flow dynamics, Figure 7 presents radial velocity at the contraction plane for Reynolds numbers varying from 2 to 100. A fully-developed parabolic profile at the contraction plane is obtained for  $Re=2$ . The Reynolds number growth gives rise to quasi-uniform velocity profiles at the symmetry line subject to severe boundary layers. The most advective profile ( $Re=100$ ) presents an overshoot at boundary layer edge, which may be eliminated by employing a shock-capture strategy (Galeão and Carmo, 1988).

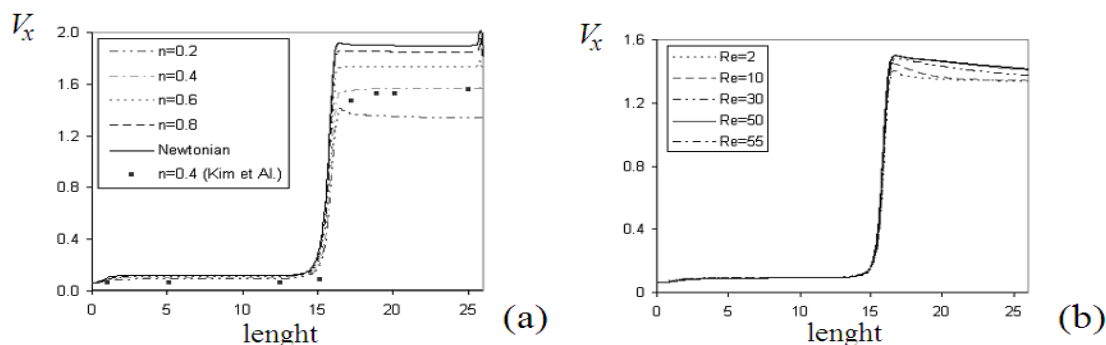


Figure 8: Axial velocity profiles along symmetry axis for  $Cu=100$ : (a)  $Re=2$  and distinct power-law coefficients; (b)  $n=0.2$  and distinct Reynolds numbers. Comparison 9-11

Figure 8 investigates the influence of the power-law coefficient (ranging from  $n=0.2$  to  $n=1.0$ ) and the inertia influence (with Reynolds number varying from 2 to 55) on the axial velocity profiles along symmetry axis, considering a high value of Carreau number – namely  $Cu=100$ . Figure 8(a) has been obtained by neglecting inertial effects, for  $Re=2$ . At the larger tube (a low shear rate region) the velocity profiles are almost independent from the power-law coefficient; otherwise, at the smaller one, the velocity profile suffers a strong influence of the power-law coefficient. As it may be noticed, at the latter region the velocity values decrease as  $n$  decreases. A comparison between the present work results for  $n=0.4$  and those by Kim *et al.* (1983) is also presented in Figure 8(a), both results showing a very good agreement, but in the vicinity of the contraction plane.

Figure 8(b) illustrates the inertia effects on the axial velocity profiles along the symmetry axis, for the most shear-thinning case ( $Cu=100$  and  $n=0.2$ ) with Reynolds number varying from 2 to 55. This figure reveals an almost negligible influence of Reynolds number on the velocity profiles. In the larger tube, even for the smaller Reynolds value ( $Re=2$ ), the flow is advective-dominated due to the high value of the shear-thinning coefficient ( $n=0.2$ ) – as indicated by the overlapping of all curves. Yet in the smaller tube one may notice a differentiation of the curves with the increase of Reynolds number. As Reynolds grows, one may observe only a small augmentation of the centerline velocities due to the very low value of the shear-thinning coefficient of the fluid ( $n=0.2$ ).

## 5. FINAL REMARKS

A Galerkin least-squares finite element formulation has been employed to approximate an isochoric Carreau flow through an axisymmetric sudden contraction, with the results being successfully compared to those by Kim *et al.* (1983). It was verified that the increase of shear-thinning effect causes a strong influence on the flow dynamics. The velocity profiles at the contraction plane become high advective-dominated with the increase of the shear-thinning coefficient and the increase of the Carreau number, with the presence of a strong boundary layer near the pipe wall. As shear-thinning increases, three distinct behaviors were verified in this article: the velocity profiles at the contraction plane become flatter; the vortex size at the contraction corner decreases until its collapse and the pressure drop along the flow suffers a strong reduction.

## 6. ACKNOWLEDGEMENTS

The author F. Silveira thanks for its undergraduate scholarship provided by FAPERGS. Author S. Frey acknowledges CNPq and author M. L. Martins-Costa acknowledges CNPq and FAPERJ, for financial support and grants.

## 7. REFERENCES

- Bird, R. B. Armstrong, R. C. Hassager, O., 1987, “Dynamics of polymeric liquids”. v.1, John Wiley & Sons, U.S.A.  
 Ciarlet, P.G., 1978, “The finite element method for elliptic problems”, North-Holland, Amsterdam.

- Fang, P., Manglik, R.M. and Jog, M.A., 1999. "Characteristics of laminar viscous shear-thinning fluid flows in eccentric annular channels", *J. Non-Newt. Fluid Mech.*, vol. 84, pp. 1-17.
- Franca, L.P., and Frey, S., 1992, "Stabilized finite element methods: II. The incompressible Navier-Stokes equations", *Comput. Methods Appl. Mech. Engrg.*, vol. 99, pp. 209-233.
- Galeão A. C., do Carmo E. G. D., 1988. "A consistent approximate upwind Petrov-Galerkin method for convection-dominated problems", *Comput. Method Appl. Mech. Engrg.*, vol. 68, pp.83-95.
- Ghia, U., Ghia, K.N., and Shin, C.T., 1982, "Hi-Re solution for incompressible flow using the Navier-Stokes equations and the multigrid method", *J. Comput Physics.*, vol. 48, pp. 387-411.
- Jurjevic, R., 1999, "Modelling of two-dimensional laminar flow using finite element method", *International Journal for Numerical ethods in Fluids*, vol. 31, pp. 601-626.
- Kim, M.E., Brown, R.A., Armstrong, R.C., 1983, "The roles of inertia and shear-thinning in flow of an inelastic liquid through an axisymmetric sudden contraction", *Journal of Non-Newtonian Fluid Mechanics*, vol. 13, pp. 341-363.
- Neofytou, P., 2005, "A 3rd order upwind finite volume method for generalized Newtonian fluid flows", *Journal of Non-Newtonian Fluid Mechanics*, vol. 36, pp. 664-680.
- Reis Junior, L.A., and Naccache, M.F., 2003, "Analysis of non-Newtonian flows trough contractions and expansions", *XVII Congresso Brasileiro de Engenharia Mecanica*, Sao Paulo/SP. vol. 1.

## 8. RESPONSIBILITY NOTICE

The authors are the only responsible for the printed material included in this paper.